ARTICLES
https://doi.org/10.1038/s41566-019-0425-3
nature photonics

Josephson vortices induced by phase twisting a polariton superfluid

Davide Caputo[1,2], Nataliya Bobrovska[3], Dario Ballarini[1*], Michal Matuszewski[3], Milena De Giorgi[1], Lorenzo Dominici[1], Kenneth West[4], Loren N. Pfeiffer[4], Giuseppe Gigli[1,2] and Daniele Sanvitto[1,5]

Quantum fluids of light are an emerging platform for energy-efficient signal processing, ultrasensitive interferometry and quantum simulators at elevated temperatures. Here we demonstrate all-optical control of the topological excitations in a large polariton condensate realizing the bosonic analogue of a long Josephson junction and inducing the nucleation of Josephson vortices. When a phase difference is imposed at the boundaries of the condensate, two extended regions become separated by a sharp phase jump of π radians and a solitonic depletion of the density, forming an insulating barrier with a suppressed order parameter. The superfluid behaviour—characterized by a smooth phase gradient across the system instead of the sharp phase jump—is recovered at higher polariton densities and is mediated by the nucleation of Josephson vortices within the barrier. Our results contribute to the understanding of dissipation and stability of elementary excitations in macroscale quantum systems.

Bose–Einstein condensation and the closely related phenomena of superfluidity and superconductivity are striking manifestations of macroscale quantum physics. The quest for practical applications has stimulated a search for systems in which superconductivity or superfluidity could be exploited in realistic devices. In the past decade, the development of new materials and heterostructures has led to the emergence of quantum fluids of light[1,2]. They are typically realized in semiconductor microcavities, which allow for the existence of peculiar states called exciton polaritons (hereafter, polaritons)[3]. In these systems, light–matter interaction is larger than dissipation and the elementary excitations cannot be described by the bare exciton and photon modes. Instead, polaritons are the eigenstates, resulting from the coherent coupling of excitons and photons. Polaritons have extremely low effective mass ($10^{-5}m_0$, where m_0 is the electron mass) and bosonic statistics, providing a suitable system in which to observe condensation in a single state even at room temperature and in a solid-state environment. Moreover, their peculiar light–matter composition allows the investigation of collective density and phase excitations with relatively simple optical setups, with the advantage of the possibility of directly measuring the velocity field from the phase gradient[4]. Recently, superfluidity has been achieved at room temperature in organic semiconductor structures[5], and analogues of short Josephson junctions have been demonstrated in inorganic microcavities[6,7].

More generally, the behaviour of a complex order parameter in proximity to a junction and the associated formation of phase slips and vortices have been central to research not only in superconducting systems, but also in superfluid helium and Bose–Einstein condensates of ultracold atoms[8–10]. In contrast to short (point-like) Josephson junctions, so-called long Josephson junctions (LJJs) are characterized by an interface that extends beyond the Josephson penetration depth in at least one dimension[11]. One of the most interesting phenomena that occur in LJJs are Josephson vortices, which, in contrast to Abrikosov or Pearl vortices, are localized within the barrier and characterized by opposite transverse supercurrents in the two superconductors[12–14]. With respect to the charged case, a bosonic Josephson vortex is characterized by the absence of a magnetic flux and its description necessarily involves both the phase and the amplitude of the wavefunction[15,16].

Here, we observe an LJJ in a system composed of two regions of polariton condensate with macroscale quantum phases controlled by additional external lasers. The junction interface extends over several tens of micrometres and forms in response to a twist of the phase of the condensate. The twist results in the creation of a dark soliton-like coherent structure, which plays the role of an insulating barrier with a reduced order parameter. By increasing the particle density, we drive the system to an instability that results in the creation of stable Josephson vortices. Finally, we show that increasing the pumping further results in the destruction of the solitonic barrier and the appearance of a single extended condensate, which is the ground state of the system, indicating the recovery of the superfluid behaviour.

Results

The sample used in our experiments is a high-quality-factor ($Q > 10^5$) semiconductor microcavity with polariton lifetimes of around 100 ps (see Methods). Similar microcavities have recently been shown to exhibit ballistic propagation in the cavity plane for hundreds of micrometres and polariton condensation outside the laser spot when confined by ad hoc trapping potentials[17–22]. Here, a two-dimensional polariton condensate, extending across a region much larger than the healing length, is excited by a continuous-wave laser that is tuned well above the polariton resonances and uses a two-step relaxation mechanism, as done in ref. [23]. In this configuration, the dephasing induced by the high exciton density in the reservoir is limited by the ability to spatially separate the condensate from the excitation spot[24]. The exciton reservoir is first populated through the relaxation of carriers generated by the non-resonant laser, increasing the energy of the polariton dispersion (energy blueshift) in the region under the excitation spot by around 4 meV (ref. [23]). Polaritons at high energy are accelerated radially outwards from the excitation spot and, through the joint effect of high

[1]CNR NANOTEC—Institute of Nanotechnology, Lecce, Italy. [2]University of Salento, Lecce, Italy. [3]Institute of Physics, Polish Academy of Sciences, Warsaw, Poland. [4]Department of Electrical Engineering, Princeton University, Princeton, NJ, USA. [5]INFN, Sezione Lecce, Lecce, Italy.
*e-mail: dario.ballarini@nanotec.cnr.it

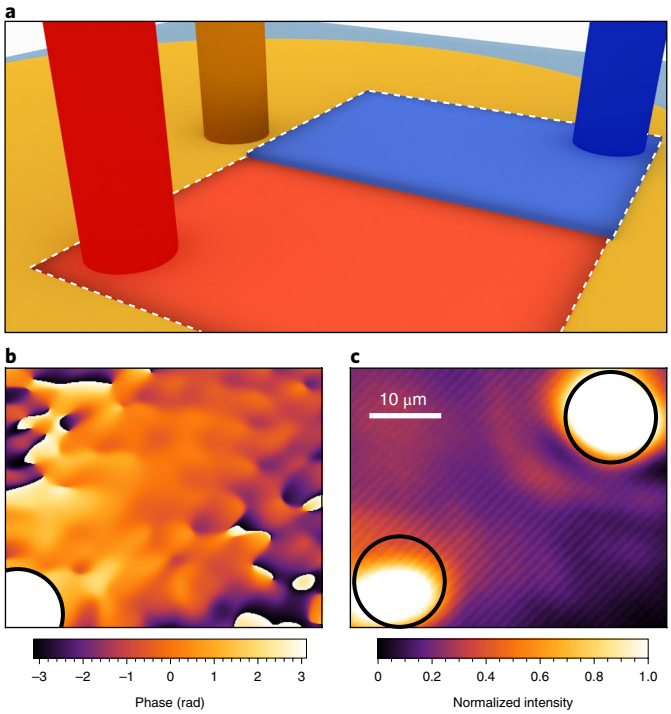

Fig. 1 | Double phase locking of the condensate via external lasers. **a**, Sketch of the polariton condensate (yellow), with the non-resonant pump shown as a dark yellow cylinder. The blue (red) region corresponds to the region in which the phase of the condensate is determined by the resonant laser beams shown as the blue (red) cylinder. The white dashed rectangle indicates the region shown in the measurements in **b** and **c**. **b**, Phase of the condensate just above the power threshold for quantum degeneracy, locked to that of the external laser in the bottom-left corner of the image. The scale bar in **c** also applies in **b**. The white circle corresponds to the saturated signal of the reflected beam. **c**, Measured interferogram of the extended condensate. The resonant beams, partially reflected at the surface, saturate the detector at the positions of the two spots (circles), despite the small number of injected polaritons.

velocity propagation and phonon-assisted relaxation, they populate the bottom state of the polariton band even at distances of hundreds of micrometres from the blueshifted region[23,25]. Eventually, stimulated scattering leads to the formation of an extended polariton condensate all around the injection spot in the ground state of the dispersion ($k \approx 0$, where k is the component of the polariton wavevector parallel to the plane of the cavity)[23]. In the sketch in Fig. 1a, a portion of the polariton condensate is highlighted by a dashed white rectangle and represents the region under consideration in the subsequent measurements. The phase $\phi(\mathbf{r})$ of the polariton condensate is obtained in two dimensions from the interference fringes between the signal emitted by the condensate and a reference with a spatially uniform phase (see Methods).

We next show that the phase of the polariton condensate can be locked to that of an external laser, acting as a seed in the symmetry-breaking process, tuned to resonance with the energy of the condensate[26,27]. This is shown in Fig. 1b, where the phase of the condensate is locked to that of an external laser beam, resonant with the condensate frequency and focused in the bottom-left corner of the image (see Methods and Supplementary Information). Note that the phase locking of the condensate is non-local: whereas the external laser is focused into a small spot (white circle in Fig. 1b) of radius $r = 5\,\mu$m and is kept at low enough power to induce only a negligible contribution to the condensate density, the phase locking extends over the whole condensate, creating a domain of uniform phase across the entire region of interest (coherence length of 50–100 μm; see Methods).

As shown in the sketch in Fig. 1a and in the experimental interferogram in Fig. 1c, we impose a twisted boundary condition on the condensate by focusing a second, resonant external beam with the same wavelength but a different phase at a distance of about 50 μm (top-right corner in the interferogram shown in Fig. 1c). Note that the healing length is one order of magnitude smaller, $\xi \approx 5\,\mu$m (ref. [24]). In contrast to the phase imprinting schemes first used with atomic condensates, in our configuration the phase is imposed at only the top-right and bottom-left corners in Fig. 1c; it is unconstrained in the region between the two phase-locking points[28,29]. When two concurrent beams with a phase difference act on the condensate, two phase domains are expected as a result of the competing phases of the locking lasers[30]. This arrangement is depicted in Fig. 1a, with the red and blue rectangles marking the two regions of uniform phase. We next measured the actual response of the condensate to the twisted boundary condition for different polariton densities.

The polariton density can be increased by increasing the power of the non-resonant pump, without changing the intensity of the two phase-locking beams. We note that our photoluminescence measurements detect the steady state of the system, averaged temporally owing to the time-integrated detection (a few milliseconds). Therefore, although the microscale evolution of the system may change in different realizations depending on possible slight variations in the initial conditions, the more stable steady-state solution is naturally captured in the experiments. When the polariton density is below the condensation threshold, $d_{\mathrm{th}} \approx 0.5$ polaritons μm^{-2}, a macroscale phase is not defined in the region between the two resonant beams and the phase fluctuates from point to point (Fig. 2a). In Fig. 2e, the unwrapped phase profiles along the vertical direction in the black rectangle in Fig. 2a show the random phase oscillations in space. In Fig. 2b–d, the polariton density is brought above the condensation threshold, allowing the double locking of the condensate. For densities $d \approx 1.5 d_{\mathrm{th}}$, the hierarchy of excitations induced by the phase imprinting (phase difference of $\delta\phi \approx \pi$) results in two regions of the condensate being neatly separated by a wavy junction for about 30 μm, as shown in Fig. 2b. The phase profile across the junction (Fig. 2f) shows a steep phase jump of $\Delta\phi \approx \pi$, with a corresponding depletion in the density profile (green line in Fig. 2i), demonstrating the spontaneous appearance of a dark soliton-like structure that acts as an insulating barrier.

In analogy to what has been observed in atomic Bose–Einstein condensates[28], optical nonlinear waves[31] and one-dimensional polaritonic wires[32], the formation of a soliton is an expected consequence of the imposed phase boundary condition[30]. However, even if the topological nature of the junction could partially explain the relative robustness of this configuration against noise, in two-dimensional systems, transversal modulation instabilities (snake instabilities) transform dark solitons into vortex–antivortex pairs, vortex rings, vortex dipoles or even more complex dynamics[33–36]. The spontaneous formation and stability of such a topological excitation are notable consequences of this phase-imprinting scheme in driven dissipative systems.

For increasing densities ($d \approx 2.0 d_{\mathrm{th}}$), the solitonic junction is still present but the phase difference is inverted at some points along the nodal line (Fig. 2c). The presence of vortices and regions with inverted currents is captured by the opposite π shift of the phase in Fig. 2g. Eventually, at the highest pumping powers used in our experiments, the junction completely disappears, leaving a shallow phase gradient across the condensate (Fig. 2d,h). At these densities ($d \approx 2.5 d_{\mathrm{th}}$), the phase stiffness is enough to avoid phase jumps and density depletions, recovering the superfluid behaviour in the region under consideration[30].

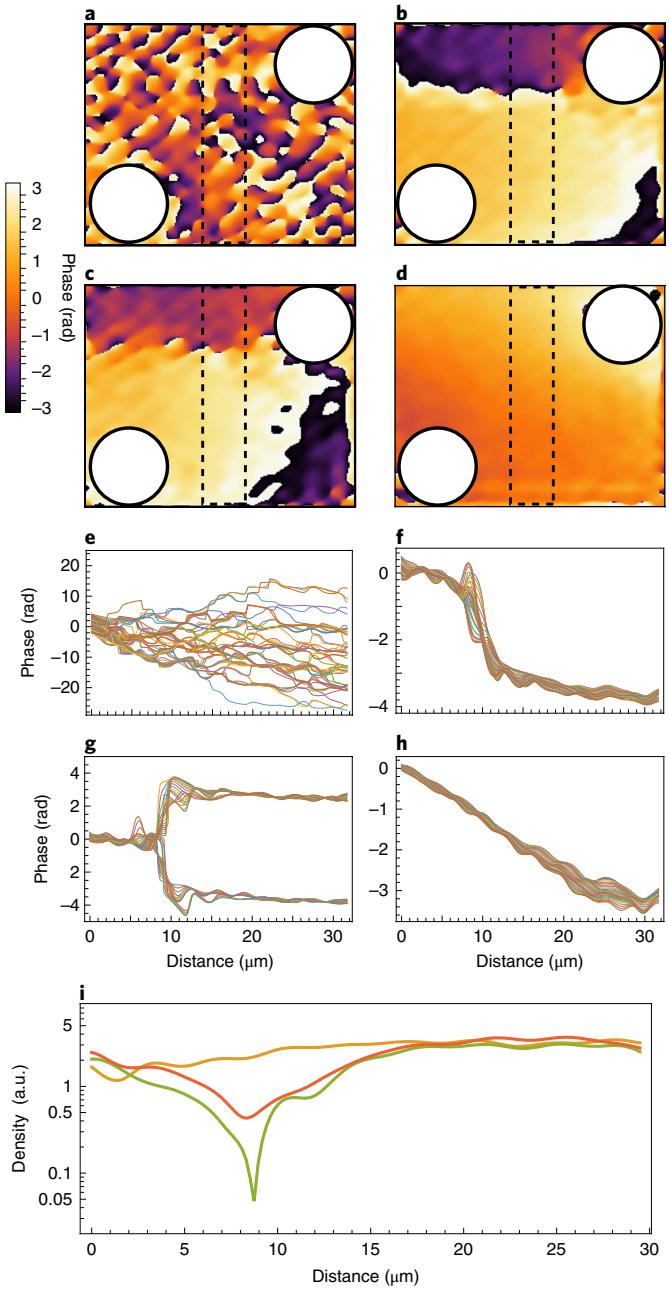

Fig. 2 | Phase and density of the condensate on phase twisting. a–d, Phase (mod 2π) of the condensate with a twisted boundary condition ($\Delta\phi=\pi$) when the intensity of the non-resonant pump is increased. **a**, $d=0.5d_{th}$. **b**, $d=1.5d_{th}$. **c**, $d=2.0d_{th}$. **d**, $d=2.5d_{th}$. The dashed rectangles correspond to 8 μm × 35 μm regions. **e–h**, Phase profiles along the vertical direction, with colours indicating different horizontal positions spanning the region within the dashed black rectangles in **a–d** with 36 lines corresponding to spatial steps of 0.22 μm. **i**, Density profiles extracted from the interferograms corresponding to the phase maps shown in **b** (green line), **c** (red line) and **d** (yellow line).

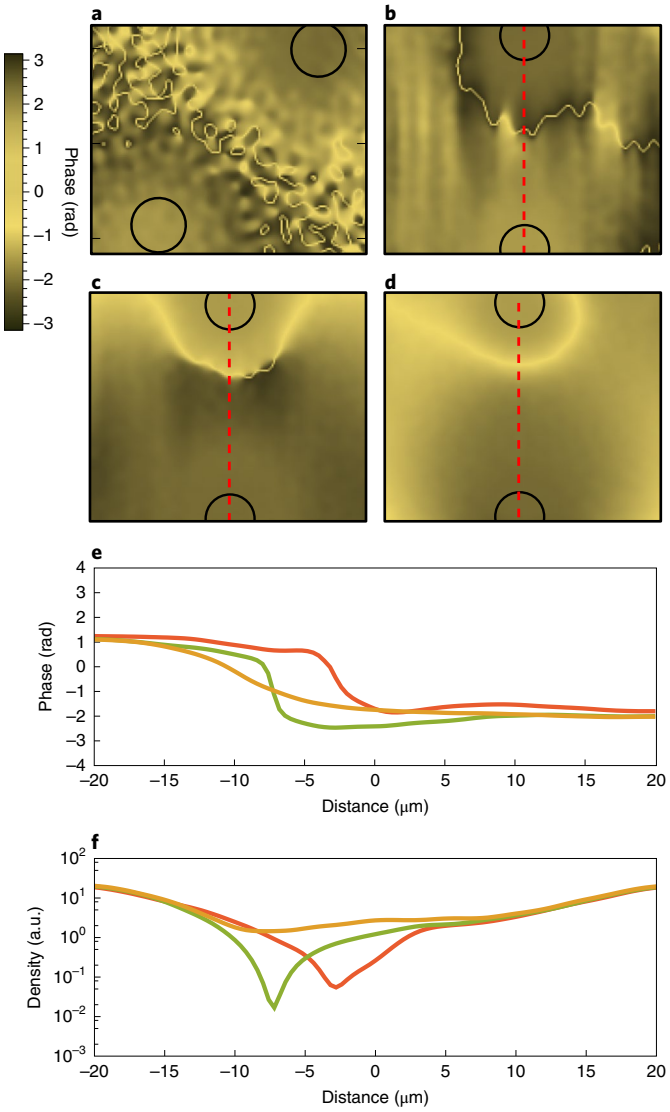

Fig. 3 | Numerical simulations. a–d, Phase profiles obtained numerically with increasing pump power. **a**, $P \ll P_{th}$. **b**, $P=4.5P_{th}$. **c**, $P=6P_{th}$. **d**, $P=8P_{th}$. Tick marks in **a** correspond to 10 μm. **e**,**f**, Cross-sections of the phase (**e**) and density (**f**) along the red dashed lines in **b** (green lines), **c** (red lines) and **d** (yellow lines). Note that in **b–d** the orientation of the cross-section with respect to the pumping spots was chosen so that it is approximately perpendicular to the barrier.

We reproduce numerically these stages of formation and disappearance of coherent structures using the complex Ginzburg–Landau equation, adapted to the case of a polariton condensate separated from the exciton reservoir[24] (see Methods). In Fig. 3a–d we show the results of simulations carried out with increasing pump power, qualitatively reproducing the formation of a solitonic barrier, the nucleation of vortices and finally the appearance of a homogeneous condensate. The figures show snapshots of the phase of the wavefunction after a long time of evolution, when the initial transient effects have washed out and the system has approached the steady state. Cross-sections of the phase and density profiles are shown in Fig. 3e,f. We find that the formation of the barrier and vortices observed experimentally is reproduced in simulations. The phase jumps imprinted by the pump, together with the noise present in the stochastic equation, act as a seed for the appearance of solitons and vortices. In the experiment, the noise is not stochastic but due to very small local fluctuations of the photonic or exciton potential[37]. In the absence of disorder potential in the simulation, the positions of the solitons and vortices fluctuate. However, we find numerically that a weak static disorder is able to pin the topological excitations in certain fixed positions, without altering their physical structure, exactly as happened in the experiment. At the same time, the potential disorder required for pinning is very weak and by itself

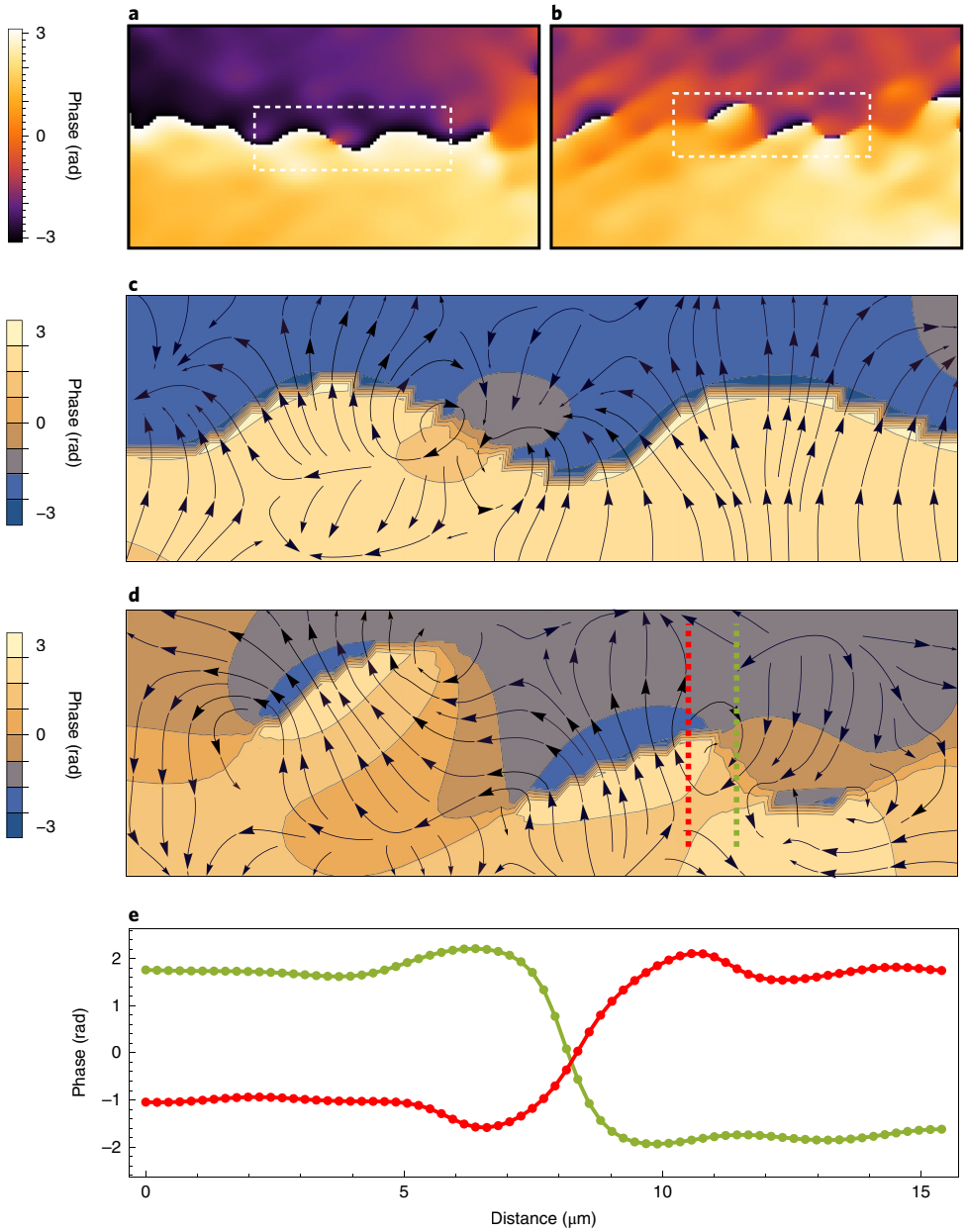

Fig. 4 | Josephson vortices nucleation at the long Josephson junction. a,**b**, Detail of the regions with the phase jump in Fig. 2b,c, respectively, with the appearance of a wavy junction. The areas shown by the white dashed rectangles are 5 μm × 15 μm. **c**,**d**, Velocity streamlines directly obtained as the two-dimensional gradient of the phase from the experimental data in the dashed white rectangles in **a** and **b**, respectively. The arrows indicate the direction of the polariton currents, but the length does not indicate the intensity of the velocity field, which decreases away from the junction. The background images are the experimental phase data shown in the dashed white rectangles in **a** and **b**. The two-dimensional contour plot representation is used to show the velocity streamlines orthogonal to the isophase lines. **c**, The nucleation of a vortex–antivortex pair. **d**, The velocity streamlines show the proliferation of Josephson vortices (2–3 vortex–antivortex pairs are visible). The vortex between the dotted lines is an example with clockwise rotation. **e**, Phase profiles along the dashed lines in **d**, showing the inverted currents around the Josephson vortex. The whole vertical extension of 15 μm, as in **a** and **b**, is given.

does not form an insulating barrier. Phase defects appear only when the double locking is applied, otherwise a constant phase across the whole region is observed (see Supplementary Information). Since we do not assume any particular form of disorder in the simulation, the soliton is not pinned to the same point in the sample as in the experiment; its position is instead determined by a particular realization of the noise and disorder, which vary from one simulation to another.

In Fig. 4, we focus on the region in proximity to the junction for the intermediate power regime. The phase shown in Fig. 2b,c is magnified in Fig. 4a,b, respectively. The velocity vector field can be obtained directly from the measured phase $\phi(\mathbf{r})$ by $\mathbf{v}(\mathbf{r}) \propto \nabla\phi(\mathbf{r})$ (refs. [4,38,39]). The velocity streamlines corresponding to the data in the white dashed rectangles in Fig. 4a,b are shown in Fig. 4c,d, respectively. In analogy to the formation of Josephson vortices in superconducting Josephson junctions or in atomic Bose–Josephson junctions[12,13], the nucleation of vortices in the barrier allows a partial dissipation of the energy stored in the twisted-phase configuration. This is markedly different from previous work on solitons and vortices in polariton superfluids, in which hydrodynamic effects

across the condensate prevail over the dynamics of Josephson vortices within the barrier[40–42]. The appearance of the first couple of Josephson vortices is evident in Fig. 4c, where a vortex–antivortex pair (formed by vortices with opposite circulation) nucleates within the barrier and supports an inverted current going downwards (centre of Fig. 4c), as opposed to the upward flux seen across the rest of the junction.

At higher densities, the separation between the vortex and the antivortex increases and the nodal line breaks at different points (as shown in Fig. 4d), developing polariton currents in opposite directions across the junction. The solitonic features in the density and phase profiles are still visible, but now the nodal line has a more complex structure (Fig. 4d). As shown in Fig. 4e, the phase slip is inverted along the red and green dashed lines in Fig. 4d, going from $\Delta\phi \approx \pi$ to $\Delta\phi \approx -\pi$ in accordance with the inverted currents in nearby domains of the junction. Moreover, transversal currents induced by the vorticity are visible in the condensate on both sides of the junction, which now acquires a more tortuous path, with additional phase modulations departing from the vortex cores at finite angles from the main nodal line. At higher densities, all these topological excitations disappear and the system is left in a clean superfluid phase with a smooth phase gradient between the boundaries.

Discussion

The phenomenology of the transition from a solitonic structure to vortex pairs may appear similar to the transverse (snake) instability of dark solitons observed in several nonlinear two-dimensional systems[33,43–45]. However, we emphasize that our observations are not an example of such an instability, since the observed structures are stable at all values of the pumping power tested. Snake instabilities in conservative systems develop over time, evolving from an elongated dark soliton state that is prepared intentionally, for example, by careful phase imprinting. The fragility of a soliton solution of the nonlinear Schrödinger equation results in unavoidable decay into vortex–antivortex pairs, even when a phase difference is imposed as a boundary condition. The vortices that result from a snaking instability follow a dynamical evolution, moving away from the initial position, which results in a complete decay of the solitonic structure after a certain amount of time. By contrast, in our pumped dissipative system, resonant lasers provide effective phase locking, which results in a stable two-dimensional solitonic structure. At higher pump power, the soliton splits into vortex pairs that stay close to the initial soliton dip, and the insulating character of the barrier is partially retained, as can be seen from the phase profiles in Figs. 2g and 4e. Moreover, the last stage of the transition shown in Fig. 2d, with a smooth phase and flat density, is never observed as a result of an instability in a conservative system. This can be understood in the following way. The increase in pumping drives our non-equilibrium condensate to lower energy states as a result of faster thermalization[46]. This leads to the transition from the soliton-like state, through the proliferation of vortices, to the flat density state that is closest to the ground state of the system (see Methods for a detailed calculation of the energy of particular states). Hence, the transition from the solitonic state to vortices to a flat state is a result of gradual relaxation between stable steady states, rather than an instability of an artificially prepared out-of-equilibrium state that decays unavoidably. From the point of view of potential applications, the stability of these steady states is a considerable advantage over unstable states.

In conclusion, we have shown the full range of dynamical responses of a polariton condensate to a twisted-phase boundary condition by changing the polariton density and looking at the steady-state evolution of the system. The existence of a stable spatial soliton with a wavy nodal line, as in Fig. 2b, is a remarkable topological feature and constitutes a natural realization of a bosonic LJJ in polariton condensates[47]. The solitonic structure is characterized by a strong reduction of the order parameter (condensate wavefunction amplitude), which acts as an analogue of the normal barrier, or weak link, in superconducting Josephson junctions, and separates two extended regions of the condensate with well-defined phases. The transition from the superfluid behaviour to the formation of stable topological excitations can be controlled in the same experiment by optically tuning the polariton density, suggesting the possibility of testing the scaling laws of interacting quantum fluids[48] in a solid-state environment.

Online content

Any methods, additional references, Nature Research reporting summaries, source data, statements of code and data availability and associated accession codes are available at https://doi.org/10.1038/s41566-019-0425-3.

Received: 10 May 2018; Accepted: 26 March 2019;
Published online: 6 May 2019

References

1. Carusotto, I. & Ciuti, C. Quantum fluids of light. *Rev. Mod. Phys.* **85**, 299–366 (2013).
2. Sanvitto, D. & Kéna-Cohen, S. The road towards polaritonic devices. *Nat. Mater.* **15**, 1061–1073 (2016).
3. Kasprzak, J. et al. Bose–Einstein condensation of exciton polaritons. *Nature* **443**, 409–414 (2006).
4. Nardin, G. et al. Hydrodynamic nucleation of quantized vortex pairs in a polariton quantum fluid. *Nat. Phys.* **7**, 635–641 (2011).
5. Lerario, G. et al. Room-temperature superfluidity in a polariton condensate. *Nat. Phys.* **13**, 837–841 (2017).
6. Lagoudakis, K. G., Pietka, B., Wouters, M., André, R. & Deveaud-Plédran, B. Coherent oscillations in an exciton-polariton Josephson junction. *Phys. Rev. Lett.* **105**, 120403 (2010).
7. Abbarchi, M. et al. Macroscopic quantum self-trapping and Josephson oscillations of exciton polaritons. *Nat. Phys.* **9**, 275–279 (2013).
8. Sukhatme, K., Mukharsky, Y., Chui, T. & Pearson, D. Observation of the ideal Josephson effect in superfluid ^{4}He. *Nature* **411**, 280–283 (2001).
9. Tanzi, L. et al. Velocity-dependent quantum phase slips in 1D atomic superfluids. *Sci. Rep.* **6**, 25965 (2016).
10. Abad, M. et al. Phase slips and vortex dynamics in Josephson oscillations between Bose-Einstein condensates. *Europhys. Lett.* **109**, 40005 (2015).
11. Barone, A. & Paterno, G. *Large Junctions—Static Self-Field Effects* 96–120 (John Wiley & Sons, 2005).
12. Kaurov, V. M. & Kuklov, A. B. Josephson vortex between two atomic Bose-Einstein condensates. *Phys. Rev. A* **71**, 011601 (2005).
13. Roditchev, D. et al. Direct observation of Josephson vortex cores. *Nat. Phys.* **11**, 332–337 (2015).
14. Yoshizawa, S. et al. Imaging Josephson vortices on the surface superconductor Si(111)-($\sqrt{7}\times\sqrt{3}$)- In using a scanning tunneling microscope. *Phys. Rev. Lett.* **113**, 247004 (2014).
15. Kaurov, V. M. & Kuklov, A. B. Atomic Josephson vortices. *Phys. Rev. A* **73**, 013627 (2006).
16. Abad, M., Guilleumas, M., Mayol, R., Pi, M. & Jezek, D. M. Phase slippage and self trapping in a self induced bosonic Josephson junction. *Phys. Rev. A* **84**, 035601 (2011).
17. Nelsen, B. et al. Dissipationless flow and sharp threshold of a polariton condensate with long lifetime. *Phys. Rev. X* **3**, 041015 (2013).
18. Steger, M. et al. Long range ballistic motion and coherent flow of long lifetime polaritons. *Phys. Rev. B* **88**, 235314 (2013).
19. Sun, Y. et al. Bose-Einstein condensation of long-lifetime polaritons in thermal equilibrium. *Phys. Rev. Lett.* **118**, 016602 (2017).
20. Wertz, E. et al. Spontaneous formation and optical manipulation of extended polariton condensates. *Nat. Phys.* **6**, 860–864 (2010).
21. Kammann, E. et al. Nonlinear optical spin Hall effect and long-range spin transport in polariton lasers. *Phys. Rev. Lett.* **109**, 036404 (2012).
22. Dreismann, A. et al. A sub-femtojoule electrical spin-switch based on optically trapped polariton condensates. *Nat. Mater.* **15**, 1074–1078 (2016).
23. Ballarini, D. et al. Macroscopic two-dimensional polariton condensates. *Phys. Rev. Lett.* **118**, 215301 (2017).
24. Caputo, D. et al. Topological order and equilibrium in a condensate of exciton-polaritons. *Nat. Mater.* **17**, 145–151 (2018).
25. Antón, C. et al. Energy relaxation of exciton-polariton condensates in quasi-one-dimensional microcavities. *Phys. Rev. B* **88**, 035313 (2013).

26. Wouters, M. Synchronized and desynchronized phases of coupled nonequilibrium exciton-polariton condensates. *Phys. Rev. B* **77**, 121302 (2008).
27. Eastham, P. R. Mode locking and mode competition in a nonequilibrium solid-state condensate. *Phys. Rev. B* **78**, 035319 (2008).
28. Denschlag, J. et al. Generating solitons by phase engineering of a Bose-Einstein condensate. *Science* **287**, 97–101 (2000).
29. Cataliotti, F. S. et al. Josephson junction arrays with Bose-Einstein condensates. *Science* **293**, 843–846 (2001).
30. Janot, A., Hyart, T., Eastham, P. R. & Rosenow, B. Superfluid stiffness of a driven dissipative condensate with disorder. *Phys. Rev. Lett.* **111**, 230403 (2013).
31. Swartzlander, G. A. & Law, C. T. Optical vortex solitons observed in Kerr nonlinear media. *Phys. Rev. Lett.* **69**, 2503 (1992).
32. Goblot, V. et al. Phase-controlled bistability of a dark soliton train in a polariton fluid. *Phys. Rev. Lett.* **117**, 217401 (2016).
33. Anderson, B. P. et al. Watching dark solitons decay into vortex rings in a Bose-Einstein condensate. *Phys. Rev. Lett.* **86**, 2926–2929 (2001).
34. Ma, M., Carretero-González, R., Kevrekidis, P. G., Frantzeskakis, D. J. & Malomed, B. A. Controlling the transverse instability of dark solitons and nucleation of vortices by a potential barrier. *Phys. Rev. A* **82**, 023621 (2010).
35. Verma, G., Rapol, U. D. & Nath, R. Generation of dark solitons and their instability dynamics in two-dimensional condensates. *Phys. Rev. A* **95**, 043618 (2017).
36. Gallem, A., Guilleumas, M., Mayol, R. & Mateo, A. M. Multidimensional Josephson vortices in spin-orbit-coupled Bose-Einstein condensates: snake instability and decay through vortex dipoles. *Phys. Rev. A* **93**, 033618 (2016).
37. Lagoudakis, K. G. et al. Probing the dynamics of spontaneous quantum vortices in polariton superfluids. *Phys. Rev. Lett.* **106**, 115301 (2011).
38. Dominici, L. et al. Vortex and half-vortex dynamics in a nonlinear spinor quantum fluid. *Sci. Adv.* **1**, e1500807 (2015).
39. Gianfrate, A. et al. Superluminal x-waves in a polariton quantum fluid. *Light Sci. Appl.* **7**, 17119 (2018).
40. Tosi, G. et al. Geometrically locked vortex lattices in semiconductor quantum fluids. *Nat. Commun.* **3**, 1243 (2012).
41. Hivet, R. et al. Interaction-shaped vortex-antivortex lattices in polariton fluids. *Phys. Rev. B* **89**, 134501 (2014).
42. Ohadi, H. et al. Nontrivial phase coupling in polariton multiplets. *Phys. Rev. X* **6**, 031032 (2016).
43. Mamaev, A. V., Saffman, M. & Zozulya, A. A. Propagation of dark stripe beams in nonlinear media: snake instability and creation of optical vortices. *Phys. Rev. Lett.* **76**, 2262–2265 (1996).
44. Tikhonenko, V., Christou, J., Luther-Davies, B. & Kivshar, Y. S. Observation of vortex solitons created by the instability of dark soliton stripes. *Opt. Lett.* **21**, 1129–1131 (1996).
45. Frantzeskakis, D. J. Dark solitons in atomic Bose-Einstein condensates: from theory to experiments. *J. Phys. A* **43**, 213001 (2010).
46. Lai, C. W. et al. Coherent zero-state and π-state in an exciton–polariton condensate array. *Nature* **450**, 529–532 (2007).
47. Reinhardt, W. P. & Clark, C. W. Soliton dynamics in the collisions of Bose-Einstein condensates: an analogue of the Josephson effect. *J. Phys. B* **30**, L785 (1997).
48. Su, S.-W., Gou, S.-C., Bradley, A., Fialko, O. & Brand, J. Kibble–Zurek scaling and its breakdown for spontaneous generation of Josephson vortices in Bose–Einstein condensates. *Phys. Rev. Lett.* **110**, 215302 (2013).

Acknowledgements

D.C., D.B. and D.S. acknowledge the ERC project POLAFLOW—Polariton condensates: from fundamental physics to quantum based devices (grant number 308136) and the ERC 'ElecOpteR' grant number 780757. N.B. and M.M. acknowlegde support from National Science Center grant numbers 2015/17/B/ST3/02273 and 2016/22/E/ST3/00045. The authors thank P. Cazzato for his constant help. Discussions with M. H. Szymańska are acknowledged. The work at Princeton University was funded by the Gordon and Betty Moore Foundation through the EPiQS initiative grant GBMF4420 and by the National Science Foundation MRSEC grant DMR 1420541.

Author contributions

N.B. and M.M. developed the theoretical model and ran the numerical simulations. K.W. and L.N.P. grew the semiconductor microcavity sample used in the experiments. M.D.G., L.D. and G.G. provided technical support. D.C., D.S. and D.B. designed the experiment and analysed/discussed the results. All authors contributed to the discussion of the results and to the preparation of the manuscript.

Competing interests

The authors declare no competing interests.

Additional information

Supplementary information is available for this paper at https://doi.org/10.1038/s41566-019-0425-3.

Reprints and permissions information is available at www.nature.com/reprints.

Correspondence and requests for materials should be addressed to D.B.

Publisher's note: Springer Nature remains neutral with regard to jurisdictional claims in published maps and institutional affiliations.

Methods

Sample and experimental setup. The sample is a high-quality-factor 3/2λ GaAs/(Al, Ga) As two-dimensional planar cavity, where $\lambda = 772$ nm is the wavelength of the longitudinal cavity resonance, with 12 GaAs quantum wells placed at three antinode positions of the electric field. The top (bottom) layer of the mirror (distributed Bragg reflectors) includes 34 (40) pairs of AlAs/$Al_{0.2}Ga_{0.8}As$ layers. The effective Rabi splitting of the sample is 16 meV. The cavity–exciton energy detuning depends on the spatial position; consequently, we used a point with a slightly negative value, $\delta = -2$ meV. Experiments are performed using a non-resonant continuous-wave excitation with a low-noise, narrow-linewidth Ti:sapphire laser with stabilized output frequency (M Squared Lasers) and chopped with a 4 kHz frequency and duty cycle of around 5% to avoid heating of the sample. In addition to the non-resonant pumping, a resonant laser, split into two beams and with momentum and energy matching the bottom of the lower polariton branch, is used to pin the phase of the condensate. The two resonant beams are produced in a compact interferometer and come from the same continuous-wave laser, and so have the same phase difference. The stability of the interferometer is optimized to minimize the residual uncertainty in the phase difference between the two beams, which is adjusted to be approximately π radians and can be controlled by tuning the position of the mirror in one of the two arms of the interferometer. The formation of the phase slip is robust enough to be observed even in the presence of the unavoidable fluctuations of the phase difference between the two resonant beams during the time of the experiment, without needing any active feedback for further stabilization of the phase difference. However, the stability of the topological structures quickly deteriorates when the nominal phase difference is shifted from π radians. The wavelength and the angle of incidence of the resonant beams are adjusted very carefully to match the resonance, both in energy and wavevector, of the polariton condensate. This is done by recreating the Fourier plane of the launching objective in a 4f configuration, with $f = 500$ mm the focal length of the lenses, to control the component of the wavevector parallel to the sample surface with a precision of 0.1 μm^{-1}.

The sample emission is collected and sent to a Mach–Zehnder interferometer and finally focused on the entrance slit of a charge-coupled device (CCD) camera. The polariton lifetime is determined by time-resolved photoluminescence measurements with a Ti:sapphire laser delivering 3 ps pulses with a repetition rate of 82 MHz. Polaritons are resonantly injected by tuning the frequency and angle of incidence of the beam to match the polariton resonance close to the bottom energy of the dispersion. Resonant excitation is required to prevent the radiative decay rate measurements from being affected by the bottleneck effect and the long lifetime of the excitonic reservoir. The photoluminescence signal is recorded with a streak camera with an overall time resolution of 3 ps and the mono-exponential decay allows us to easily extract a lifetime of 100 ps (refs. [18,23]).

Phase measurements. Measurements of the phase of the condensate are performed with a Mach–Zehnder interferometer, where the signal emitted by the microcavity is interfered with a reference beam of spatially uniform phase, obtained by expanding a single spatial point of the condensate, which is chosen to be far away from the region of interest. The phase difference from the reference value is extracted at each position of the condensate from the pattern of the interference fringes using the standard fast Fourier transform algorithm[24]. To demonstrate the non-local locking of the phase of the condensate by the external laser, we use the Mach–Zehnder interferometer to interfere a region of the condensate outside of the laser spot with a reference signal taken from the same laser used to pin the phase. In our configuration, the coherence of the condensate is not substantially altered by the phase locking with an external laser, leaving the coherence length unaffected, which, as shown in ref. [24], depends on only the polariton density of the condensed state. In particular, for our measurement of LJJs, we have a power-law decay of coherence with an exponent of $\alpha = 0.5$, which corresponds to a coherence length of $L_c = 50$ μm, whereas for the case of the superfluid regime the exponent is $\alpha = 0.25$, with $L_c > 100$ μm. The formation of quasi-long-range order is a prerequisite to having a polariton condensate large enough (>100 μm) to impose the phase locking with two external lasers. More details about the measurement of the power-law decay of first-order correlations in space and time, in the same sample and under the same experimental conditions, are given in ref. [24].

Numerical modelling. We model the polariton system using the stochastic complex Ginzburg–Landau equation[24]

$$i\frac{\mathrm{d}\psi}{\mathrm{d}t} = \left[-\frac{\hbar}{2m^*}\nabla^2 + g\,|\psi|^2 + V(\mathbf{r}) + i\left(\gamma - \kappa - \Gamma\,|\psi|^2\right)\right]\psi + F_1(\mathbf{r})\mathrm{e}^{-i\omega_L t} + F_2(\mathbf{r})\mathrm{e}^{-i\omega_L t + i\Delta\phi} + \frac{\mathrm{d}W}{\mathrm{d}t}$$

where $\psi(\mathbf{r}, t)$ is the complex wavefunction, m^* is the effective mass of lower polaritons, g is the interaction coefficient, V is the weak disorder of the sample, γ is the effective pumping rate, κ is the polariton loss rate and Γ is the saturation coefficient. The spatial functions F_1 and F_2 describe the Gaussian profiles of the two resonant pumping lasers, ω_L is the laser frequency and $\Delta\phi$ is the phase difference. The strength of the disorder $V(\mathbf{r})$ required for spatial pinning is chosen to be lower than other typical energy scales in the system, and its spatial correlation length is a few micrometres. The term $\mathrm{d}W$ is scaled Wiener noise with correlations

$$\langle \mathrm{d}W(\mathbf{r}, t)\mathrm{d}W^*(\mathbf{r}', t)\rangle = c_q\frac{\gamma + \kappa + \Gamma\,|\psi|^2}{\mathrm{d}V}\delta_{\mathbf{r},\mathbf{r}'}\mathrm{d}t$$

where c_q is a parameter representing the relative strength of quantum fluctuations present in the system. Since our condensate is spatially separated from the hot reservoir created by the pumping laser, we do not include a separate equation for the dynamics of the reservoir density.

The above form of the stochastic equation has been derived using perturbative Keldysh field theory[49] or the truncated Wigner approximation[1]. As we are not investigating the region close to the phase transition, we neglect the correction to the wavefunction due to the ordering of operators[24]. The values of parameters extracted from the experimentally measured dispersion are $m^* = 3.85\times10^{-5}m_e$ (m_e is the electron mass) and $\kappa = (100\,\mathrm{ps})^{-1}$. The interaction coefficient is $\hbar g = 4\times10^{-3}$ meV μm^2, the saturable nonlinearity is $\hbar\Gamma = 14\times10^{-3}$ meV μm^2, and the noise coefficient is $c_q = 0.1$. The blueshift of the condensate at threshold is $\hbar g d_{th} = 0.05$ meV, ω_L is set to the lower polariton energy at threshold, and their spatial full-width at half-maximum is 10 μm.

Energy of the condensate. Consider the energy of the condensate in the state that appears at the highest pump power, as in Fig. 2d, which is composed of kinetic and potential parts. The kinetic part is associated with the phase gradient between the pinning laser spots and the potential part is due to the repulsive polariton interaction

$$E_0 = \int\left[\frac{\hbar^2}{2m^*}\,|\nabla\psi|^2 + \frac{\hbar g}{2}\,|\psi|^4\right]\mathrm{d}\mathbf{r} \approx \left(\frac{A}{d^2} + B\right)S$$

where S is the approximate surface of the condensate, d is the distance between the phase-pinning beams, and A and B are constants.

The energy of the dark soliton-like state (Fig. 2b) is

$$\begin{aligned} E_{ds} &= \int_{soliton} E\mathrm{d}\mathbf{r} + \int_{rest} E\mathrm{d}\mathbf{r} \\ &\approx \left(\frac{A'}{w^2} - B'\right)S_{soliton} + B(S - S_{soliton}) \\ &= \left(\frac{A'}{w} - B'w\right)L + B(S - wL) \end{aligned}$$

where we integrate separately over the extent of the soliton and the rest, L is the length of the soliton, w is its transverse width, and A' and B' are constants corresponding to the kinetic and interaction energy in the soliton region. In the limit of a thin and long dark soliton, with $x \ll d$, L and $wL \ll S$, the dominant contribution to the difference between E_{ds} and E_0 is $E_{ds} - E_0 \approx A'L/w$, which is positive. Consequently, the dark soliton state is an excited state of the system, and the state with a small constant phase gradient has lower energy.

Data availability

The raw experimental and numerical data used in this study are available from the corresponding author on reasonable request.

References

49. Sieberer, L. M., Buchhold, M. & Diehl, S. Keldysh field theory for driven open quantum systems. *Rep. Prog. Phys.* **79**, 096001 (2016).